Feasibility Study on a Hybrid Singular Value Decomposition–Gaussian Process Regression Approach for Reactor 3D Power Reconstruction

Minhyeok Bang, Junwoo Lee, and Yonghee Kim*
Korea Advanced Institute of Science and Technology
291, Daehak-ro, Yuseong-gu, Daejeon, Republic of Korea, 34141
mh_bang@kaist.ac.kr; junwoolee@kaist.ac.kr; yongheekim@kaist.ac.kr

Keywords: singular value decomposition (SVD), artificial neural networks (ANN), Gaussian process regression (GPR), small modular reactors (SMR), ex-core neutron detectors, core-exit thermocouples (CET)

1. Introduction

For reliable and safe nuclear reactor operations, monitoring the 3D power distribution is essential. Traditional surveillance methods rely on in-core self-powered neutron detectors (SPNDs), which incur substantial installation and maintenance costs. We therefore aim to reconstruct the reactor 3D power distribution solely from ex-core neutron detectors and core-exit thermocouples (CETs).

Previous works have attempted the same reconstruction using similar sensor sets, and artificial neural networks (ANNs) have achieved noticeable success in the field [1]. However, they mainly focus on prediction accuracy and, by the nature of ANNs, offer little explainability or uncertainty quantification.

This work proposes a novel hybrid architecture of singular value decomposition (SVD) and Gaussian process regression (GPR). SVD reduces the high-dimensional power distribution into a few dominant spatial modes that explain most of its variation [2], and GPR models the relationship between the sensor signals and the corresponding modal coefficients. The 3D power distribution is then reconstructed as a linear combination of the pre-calculated SVD modes and the GPR-inferred coefficients.

The GPR-SVD model is quantitatively compared not only with an ANN-SVD model but also with the pure SVD truncation method to check its viability.

2. Methodologies

2.1 Target Reactor Model

ATOM, a KAIST-developed PWR-based SMR design [3], was chosen as the target model. It comprises 69 assemblies with a 2 m active core height and 450 MWth nominal power, 32 of which are assumed to be equipped with CETs. Twelve ex-core detectors were also modelled, at four radial positions and three axial levels. Their 3D weights were taken as the product of the 2D radial weighting function (RWF) and the 1D axial shape annealing function (SAF), so that the response of the d-th detector is the weighted sum of the nodal power:

$$S_d = \sum_{i,j} \sum_{k} RWF_d(i,j) SAF_d(k) P(i,j,k) \qquad (1)$$

where $P(i,j,k)$ is the power of assembly (i,j) at axial node k. The RWF and SAF data of the SMART-660 reactor [4] were utilised, as it shares the same core dimensions (Figs. 1 and 2). The SAFs are linearly interpolated between HZP and HFP up to 450 MWth, beyond which HFP is assumed. Each CET signal was represented by the axially integrated power of the corresponding assembly. The twelve ex-core and thirty-two CET channels thus form the 44-channel sensor input of this study.

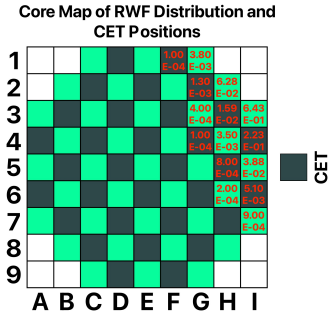


Fig. 1. Core Map of RWF Distribution and CET Locations

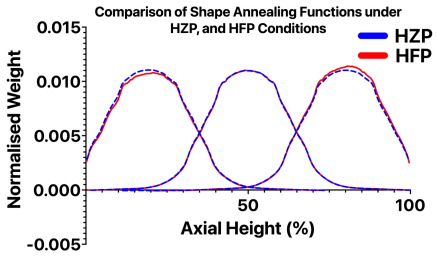


Fig. 2. Shape Annealing Functions of Ex-core Neutron Detectors

2.2 Dataset Generation

Two models, an ANN and a GPR, were trained using four time-dependent reactor transient datasets. These datasets were generated using KAIST's multi-physics PWR core simulator KANT. [5] Each scenario was

simulated for 63 hours at a 300-second interval across three different burnup conditions: BOC, MOC and EOC. This resulted in 2,271 datasets for each of the four transient cases. We then randomly sampled 80% of each dataset for training and 20% for validation. Figures 3 and 4 illustrate the characteristic power and ASI evolution for each dataset.

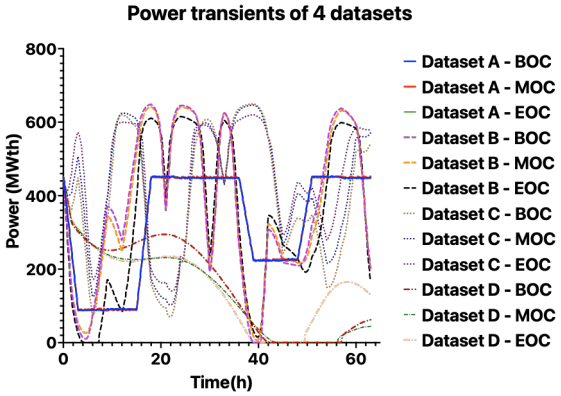


Fig. 3. Power transient evolution curves of four datasets (A, B, C, D)

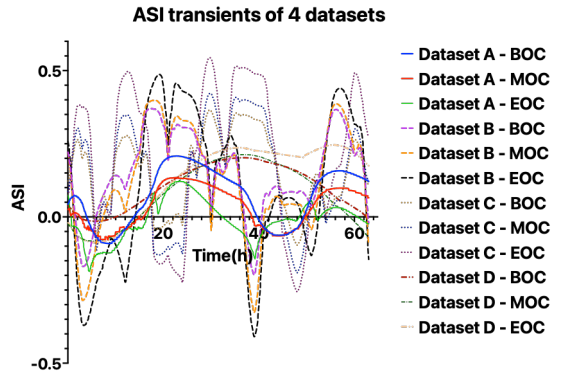


Fig. 4. ASI transient evolution curves of four datasets (A, B, C, D)

Dataset A combines 100% to 50% and 100% to 20% load-follow operations. Dataset D features all control rods inserted from 0% to 100% linearly over the entire 63% of the time. Datasets B and C are characterised by extreme transients. In dataset B, all control rods except the central bank are completely arbitrarily controlled while in dataset C every control rod bank is manoeuvred randomly. The respective position of each control rod bank is depicted in Figure 5.

2.3 SVD-Based Lower-dimension Representation of 3D Power Distributions

This study reconstructs the 3D power distribution from the 44 sensor signals (12-channel ex-core neutron detectors and 32-channel CETs). SVD is employed to make this linkage more compact and explainable by representing the power distribution with a small number of dominant spatial modes.

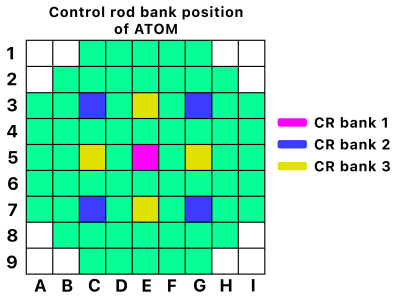


Fig. 5. Position of control rod banks in an ATOM reactor.

We can extract the dominant modes of the dataset consisting of multiple vectorised power distributions. Let $A \in \mathbb{R}^{N\times M}$ denote a data matrix whose columns correspond to vector power distributions from M operating scenarios. If we perform SVD directly on matrix A, it will naturally identify the first 'mean' mode as the dominant one. To avoid this, we subtract the mean vector $\bar{a}$ from A to create a deviation matrix A'. This matrix, A', then describes the modes of power transients over time.

$$A' = A - \bar{a}I^{\top} \tag{2}$$

Performing SVD on A′ in (1), we get,

$$A' = U\Sigma V^{\top}, \tag{3}$$

Now that we have extracted the spatial singular modes as a form of left singular vectors U, the product of the two matrices ΣV^T can then be treated as a coefficient vector, $c \in \mathbb{R}^r$ for each of the spatial modes in U, which will then be inferred by an ANN or GPR model. Then we can reconstruct a 3D power distribution a in a r-low-rank subspace, such as (4).

$$a \approx \tilde{a} + U_r c, \tag{4}$$

Having extracted the spatial singular modes as left singular vectors from multiple power distributions, we store them as an offline library of potential spatial modes for a power distribution reconstruction. This allows us to train either an ANN or GPR model to accurately infer the correct coefficient vector c for the pre-defined set of spatial modes.

2.4 Gaussian Process Regression (GPR) Model

A GPR model was used to model the relationship between the 44-channel sensor signals and the coefficient of each mode. This study assumed that each spatial mode from the SVD is independent and each singular coefficient corresponds to its own GPR model.

If we have a training set consisting of X, which are a set of sensor signals, and the corresponding SVD coefficients Y, our objective is to obtain the predictive distribution,

$$p(f_* \mid X, Y, X^*) \tag{5}$$

which describes the probabilistic distribution of SVD coefficient for unseen sensor signals, X^*.

GPR treats the unknown mapping as a random function drawn from a Gaussian process, whose covariance is governed by a kernel measuring the similarity between two inputs. The radial basis function (RBF) kernel is adopted in this study:

$$k(x_i, x_j) = \sigma_f^2 \exp\left(\frac{-\| x_i - x_j \|^2}{2l^2}\right) \quad (6)$$

where σ_f^2 is the signal variance, i.e. the prior variance of the modal coefficient, and l is the length-scale. The premise is that inputs close to each other yield strongly correlated outputs, which imposes smoothness on the inferred function.

With a zero mean function assumed in the absence of observations, the function values at the training inputs are *assumed* to follow an MVN whose covariance matrix is assembled from (6):

$$p(f \mid X) \sim \mathcal{N}(f \mid \mu, K), K_{ij} = k(x_i, x_j) \quad (7)$$

The GP assumption applies to the entire input domain, not only to the observed inputs. The value f^* at a new input X^* is therefore simply an additional element of the MVN that already contains the training values, and extending (6) to include f^* gives their joint distribution, whose covariance matrix grows by one row and one column:

$$p\begin{bmatrix} y \\ f_* \end{bmatrix} \sim \mathcal{N}\left(\begin{bmatrix} \mu(X) \\ \mu(X_*) \end{bmatrix}, \begin{bmatrix} \mathrm{K} + \sigma_n^2 I & K_* \\ K_*^T & \mathrm{K}_{**} \end{bmatrix}\right) \quad (8)$$

where $K^* = k(X, X^*)$ is the covariance between the training and the new inputs, $K^{**} = k(X^*, X^*)$ and σ_n^2 is the observation noise variance. The noise term appears only in the upper-left block to represent the observation error. Since the conditional distribution of an MVN is again an MVN, the SVD coefficient distribution sought in (5) is obtained in closed form by conditioning (8) on the observed coefficients y:

$$f_* \mid y, X, X_* \sim \mathcal{N}(\mu_*, \Sigma^*) \quad (9)$$

$$\mu_* = K_*^T (K + \sigma_n^2 I)^{-1} y \quad (10)$$

$$\Sigma^* = K_{**} - K_*^T (K + \sigma_n^2 I)^{-1} K_* \quad (11)$$

For more detailed information on GPR, readers are advised to refer to [6] which was also used as a reference for this section.

2.5 Validity Test on MVN-based Function Modelling

GPR assumes the modelled function can be represented by a multivariate normal distribution with a radial basis function covariance matrix. An ANN doesn't assume a fixed function form so validating whether a given dataset follows the presumed MVN form is crucial for GPR-based function modelling.

Let's say we have fitted a GPR model. Then the distribution of dataset is expected to follow an MVN.

$$y \sim \mathcal{N}(\mu, \mathrm{K}) \quad (12)$$

Since the covariance matrix K is positive semi-definite, we can perform Cholesky decomposition on it.

$$K = LL^{\mathrm{T}} \quad (13)$$

Now let's assume a new statistic z.

$$z = L^{-1}(y - \mu) \quad (14)$$

This z, if y follows $\mathcal{N}(\mu, K)$, should follow a standard normal distribution, as shown in (14).

$$\begin{aligned} E[z] &= E[L^{-1}(y - \mu)] \\ &= L^{-1}E[(y - \mu)] = 0 \\ cov[z] &= cov[L^{-1}(y - \mu)] \\ &= L^{-1}cov[y]L^{-1\mathrm{T}} \\ &= L^{-1}LL^{\mathrm{T}}L^{-1\mathrm{T}} = I \end{aligned} \quad (15)$$

2.6 Reference Artificial Neural Network (ANN) Model

ANNs are a natural choice for data-driven function discovery. While they lack explainability, they're incredibly powerful for regression tasks. Therefore, we selected an ANN model as a reference to evaluate how well the GPR model performs in this area.

We implemented a simple multi-layer perceptron model with three hidden layers. Each layer contained 4096, 1024 and 256 neurons respectively. LeakyReLU (a negative slope of 0.2) activation was applied throughout all hidden layers.

2.7 Reference Projection-based Pure SVD Truncation Method

A reference method was used to establish the mathematical bound of the proposed SVD low-rank representation. Unlike the ANN and GPR models, it begins with the reference 3D power distribution itself.

For a power distribution vector P_k, the best rank-r representation is the coefficient vector minimising $\|(P_k - \bar{a}) - U_r c\|_2$. Differentiating it with respect to c and setting the result to zero, with U_r orthonormal, yields:

$$U_r^{\mathrm{T}}(\mathrm{P_k} - \bar{a}) = U_r^{\mathrm{T}} U \Sigma V_k^{\mathrm{T}} = \Sigma_r V_k^{\mathrm{T}} = c_r \quad (16)$$

This is equivalent to the SVD coefficients calculated for P_k from the SVD of the entire dataset P. As (16) is L2-optimal for the given basis, the projection method is expected to show the best performance in terms of the L2 norm. However, it back-calculates the optimal coefficients from a known power distribution and cannot be used for the sensor-to-coefficient inference addressed in this study.

3. Numerical Results

3.1 Validity Test on MVN-based Function Modelling

As outlined in Section 2.5, we examined the distribution of the statistic z for each singular mode. Figure 6 illustrates a Q-Q plot for the first two modes, indicating that the SVD coefficients derived from sensor signals deviate from a standard normal distribution with some extreme cases.

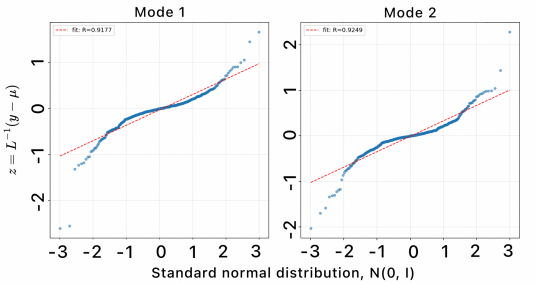


Fig. 6. A Q-Q plot of the statistic z for the first and second SVD mode coefficients

3.2 Performance benchmarks for GPR, ANN and projection methods

The three methods differ only in their SVD coefficient calculations, all utilising the same pre-calculated SVD basis vectors.

We measured the whole-core root-mean-square-error (RMSE) and the peak power absolute relative error at the actual power peak.

For the first test, we used the entire training dataset comprising all datasets (A, B, C and D) to investigate the training effectiveness of the GPR and ANN models.

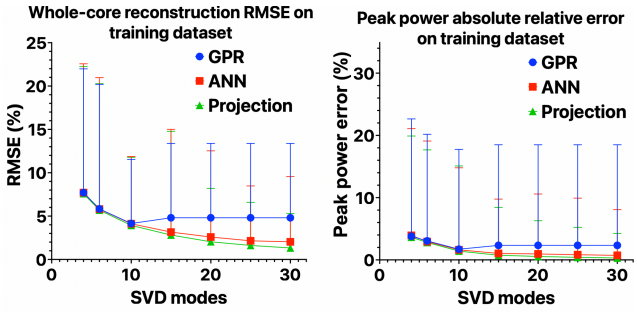


Fig. 7. Benchmark results for three methods on the training dataset.

As expected from Section 2.7, the projection method consistently offered the best performance, since its error consists solely of the rank-r truncation error while the ANN and GPR reconstructions additionally carry the coefficient-inference error.

Interestingly, while the ANN accuracy improved with more SVD modes, GPR declined beyond 10 modes, widening the gap between the two. Of the validation datasets tested, only Dataset C, which showed the poorest performance, is reported here for brevity.

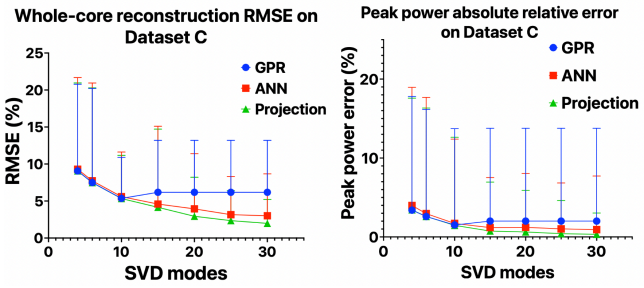


Fig. 8. Benchmark results for three methods on Dataset C

Figure 8's benchmark results demonstrate similar trends to those in Figure 7, which presented training dataset results.

The three methods differ in computational cost. The projection method requires only a matrix-vector product, though it is not deployable as noted in Section 2.7. ANN training scales as $O(N \cdot E \cdot W)$— linear in N for a given architecture — whereas GPR requires an $O(N^3)$ Cholesky factorisation of the $N \times N$ covariance matrix.

4. Conclusions and Future Works

This study proposes a novel hybrid SVD-GPR approach for reconstructing the 3D power distribution in nuclear reactors. While GPR did not outperform ANN, the framework demonstrates feasibility. Future work includes statistical analysis of the MVN-RBF function modelling, GPR hyperparameter and SVD mode optimisation, and the propagation of GPR-based coefficient uncertainty to the overall 3D power distribution.

ACKNOWLEDGEMENT

This work was supported by Korea Hydro & Nuclear Power Co., Ltd. (No. 2025-AI-001-01).

REFERENCES

[1] Li W. et al., Core power distribution reconstruction using artificial neural networks, *Nucl. Eng. Technol.*, 54 (2022) 617–626.

[2] Urase Y. et al., POD-based in-core power distribution reconstruction using ex-core detectors for HTGRs, *J. Nucl. Sci. Technol.*, 2025.

[3] Jeong Y. et al., Load-follow operation capability of soluble boron-free SMR ATOM, *Front. Energy Res.*, 13 (2025) 1639569.

[4] Roh G. et al., Ex-core detector response evaluation of the SMART reactor using DORT, *J. Nucl. Sci. Technol.*, 45 (2008) 78–81.

[5] Oh T. et al., Development and validation of the multiphysics PWR core simulator KANT, *Nucl. Eng. Technol.*, 55 (2023) 2230–2245.

[6] Wang, Jie. "An intuitive tutorial to Gaussian process regression." *Computing in Science & Engineering* 25.4 (2023): 4-11.